Determination of the thermo-optic coefficients and the thermal conductivities of a ferrofluid-doped lyotropic nematic liquid crystal using a nonlinear optical technique

S. L. Gómez and A. M. Figueiredo Neto
Instituto de Física, Universidade de São Paulo, Caixa Postal 66318, 05315-970 São Paulo, SP, Brazil
(Received 7 January 2000)

Nonlinear optical measurements are performed with a ferrolyotropic calamitic nematic mesophase with different relative concentrations of the mixture compounds. The frontiers of the nematic domain are determined using optical microscopy and x-ray scattering techniques. The thermal lens model is used to obtain the thermo-optic coefficients and the thermal conductivities of the liquid crystals. The anisotropies of these nonlinear parameters are discussed with respect to the local order and microscopic structure of the nematic phase in different positions of the N_c domain.

PACS number(s): 61.30.−v, 42.65.−k, 78.20.Ci

I. INTRODUCTION

The study of nonlinear optical phenomena in condensed matter gives to physicists and engineers an interesting field of research. In addition to the fundamental aspect of this research, many technological applications have been developed in this area, and the interest in the scientific investigation of the nonlinear properties of materials increases each year. The nonlinear optical response of thermotropic liquid crystals has been extensively studied [1–3]. In particular, the nonlinear variation of the index of refraction (n) of a material is associated with different origins: the optical Kerr effect, third order (and higher order) nonlinear electronic polarization, thermal effects, etc. [1]. Each of these processes has a characteristic response time, ranging from picoseconds to milliseconds.

One of the most simple and elegant methods to measure the nonlinear response of a medium is the *Z*-scan technique [4]. Sheik-Bahae *et al.* used this technique to obtain the nonlinear refractive index (n_2) assuming that $n=n_o+n_2I$, where n_o is the linear index of refraction and I the incident light intensity on a sample. In their approach, which is essentially *local*, changes in the electronic polarizability are responsible for the nonlinear response of the medium. Depending on the experimental conditions and on the sample absorption properties, thermal nonlinearities must be taken into account in actual *Z*-scan experiments, especially on a time scale of milliseconds. Thermal processes are due to the liquid crystal light absorption or to the presence of impurities which can also absorb heat. These processes give rise to a nonlinear response due to sample temperature changes. As a consequence, the physical properties of the liquid crystal change, affecting the propagation of the light beam itself. One of the most important effects is due to the spatial variation of the refractive index of the medium and is often referred to as *thermal lens* [5–10]. In this approach, which is essentially *nonlocal*, the index of refraction of the medium illuminated by a laser beam is written as $n=n_o+(dn/dT)\Delta T$, where T and dn/dT are the temperature and the thermo-optic coefficient.

To improve the light absorption by thermotropic liquid crystals, dyes are often mixed in with them [11,12]. On the other hand, in the case of lyotropic liquid crystals, ferrofluids [13] are used to improve their orientation in a small magnetic field [14,15], and can also absorb energy from a laser beam, heating the liquid crystal [16].

In a previous work [16] we reported on measurements of the nonlinear refractive indices of a ferrofluid-doped lyotropic liquid crystal mixture in the millisecond range using the *Z*-scan technique. On this time scale the nonlinear optical response is expected to be of thermal origin. The first approach was to fit those results to Sheik-Bahae *et al.*'s model [4] to obtain an effective n_2. In this paper we present *Z*-scan measurements performed in ferrolyotropic calamitic nematic mesophases at a fixed temperature, but with different relative concentrations of the mixture compounds. The thermal lens model (TLM) will be used to obtain the nonlinear parameters (dn/dT and the thermal conductivities) of the liquid crystals. The paper is organized as follows: Sec. II summarizes the theoretical aspects considered. Section III gives the details of the samples and the setup. The results are presented and discussed in Sec. IV. Finally, the conclusions are presented in Sec. V.

II. THEORY

In this section we will summarize the basic equations that describe the thermal lens model. The details about the model can be found in Refs. [5–10]. Consider a cw (continuous wave) Gaussian laser beam of power P (watts) incident on a weakly absorbing medium, starting at time $t=0$. The energy absorbed by the sample is immediately converted into heat. The continuous heat transfer to the sample results in the formation of a radial temperature profile. The higher temperature region is located in the center of the beam ($r=0$, where r is the radial distance from the beam axis). The index of refraction as a function of r and t is given by

$$n(r,t)=n_o+[dn/dT]\Delta T(r,t). \tag{1}$$

It is assumed that there is no convection, and that the heat axial flow is negligible. In the steady-state regime, a radial temperature gradient is established. Solving the heat conduction equation and calculating the light transmittance in the far field on the axis of the beam, we obtain the theoretical

expression for a *Z*-scan measurement. Depending upon the order of the expansion in r of the temperature field, different models can be obtained. We will focus our attention on the parabolic lens model [8]. The normalized transmittances (S) obtained with the parabolic lens model (without aberration) in a *Z*-scan experiment are

$$S_{parab}(z)=\frac{\Gamma(z,0)-\Gamma(z,\Delta t)}{\Gamma(z,\Delta t)}=\theta\left(\frac{2x}{1+x^2}\right)+\theta^2\left(\frac{1}{1+x^2}\right), \tag{2}$$

where

$$\theta=2.303P\left(-\frac{dn}{dT}\right)\frac{\alpha}{\lambda k}. \tag{3}$$

α is the linear absorption coefficient of the sample (cm^{-1}), λ is the laser wavelength (cm), k is the thermal conductivity ($\mathrm{cal\,s^{-1}\,cm^{-1}\,K^{-1}}$), Γ is the absolute (detected) transmittance, $x=z/z_o$, z_o is the confocal parameter, and Δt is the laser pulse width.

At a particular position z, the time dependence of $\Gamma(z,t)$ can be written as

$$\Gamma_{parab}(z,t)=\Gamma(z,0)\left\{1+\frac{\theta}{1+t_c/2t}\left(\frac{2x}{1+x^2}\right)+\left[\frac{\theta}{1+t_c/2t}\right]^2\left(\frac{1}{1+x^2}\right)\right\}^{-1}, \tag{4}$$

where $t_c=w^2\rho C_p/(4k)$, ρ and C_p being the density ($\mathrm{g\,cm^{-3}}$) and the sample specific heat ($\mathrm{J\,g^{-1}\,K^{-1}}$) respectively.

In a *Z*-scan experiment, from the normalized transmittance, the time evolution of the detected signal [17] and the knowledge of α, it is possible to determine the thermo-optic coefficient and the thermal conductivity.

III. EXPERIMENT

The lyotropic liquid crystal studied is a mixture of potassium laurate (KL), 1-decanol (DeOH), and water with different relative concentrations (Table I). Potassium laurate was synthesized from lauric acid (Merck), and recrystallized three times in absolute ethanol (Merck). DeOH (from Fluka, purity p.a. >98%) was purified by freezing, and the water was distilled and deionized. The errors in weighting are evaluated to be less than 0.5%. Samples were prepared and left at rest for about three days at room temperature ($T=23\,^\circ$C), before being used in the experiments. Figure 1 shows the region of the phase diagram investigated. This mixture presents a calamitic nematic phase domain (N_c) at $T=23\,^\circ$C, and all the measurements are performed at this temperature. The frontiers of this calamitic region are identified with the label *F* in Fig. 1. Different phases are present in the N_c frontiers: L_α, ISO, BIP, and N_d are the lamellar, isotropic, two-phase-region (L_α and ISO) and discotic nematic phases, respectively. These phases are identified by optical microscopic (texture observations and conoscopic measurements) and x-ray diffraction techniques. The N_c samples in the phase diagram are chosen in such a way as to keep constant the mass fraction (mol %, hereafter represented by [ ]) of DeOH (direction $A\rightarrow C$), water (direction $A\rightarrow D$) or KL (direction $A\rightarrow B$). The chemical and thermal stability of the samples were checked by measuring the optical birefringence as a function of temperature on consecutive days after the sample's preparation. After at least ten days of sample preparation, both the birefringence and the transition temperatures do not present changes larger than about 0.1% in their values. A small amount ($\sim 1.4\times 10^{13}$ grains/ml) of a surfacted water-based ferrofluid (from Ferrofluidics Corp.) is added to the mixtures with the double aim to improve the light absorption and alignment of the nematic sample in a magnetic field. The magnetic grains are made of Fe_3O_4, with mean diameter of 154 Å (standard deviation of 94 Å), double coated with oleic acid. The liquid crystal is encapsulated in rectangular glass cells 200 μm thick. Initially, the sample is oriented in a static magnetic field in an electromagnet ($H_1\sim 10$ kG). In this configuration, the sample in the nematic (N_c) phase orients in a planar geometry, with the director parallel to H_1. After that, the sample is placed in a *Z*-scan apparatus where a magnetic field (from permanent magnets)

TABLE I. Compositions of the different samples in mol %. Mixtures *A*, *B*, *C*, *D*, *AB*, *AC*, and *AD*, present a calamitic nematic phase (N_c) at $T=23\,^\circ$C. Mixtures denoted by *F* are the frontiers of the N_c domain.

Sample ↓	KL (mol %)	DeOH (mol %)	water (mol %)
A	3.14	1.20	95.66
AB	3.13	1.15	95.72
AC	3.19	1.20	95.61
AD	3.18	1.14	95.68
B	3.11	1.10	95.79
C	3.23	1.21	95.56
D	3.22	1.08	95.70
F_1	3.08	1.29	95.63
F_2	3.16	1.30	95.54
F_3	3.25	1.28	95.47
F_4	3.28	1.21	95.51
F_5	3.27	1.00	95.73
F_6	3.11	1.07	95.82
F_7	3.06	1.19	95.75

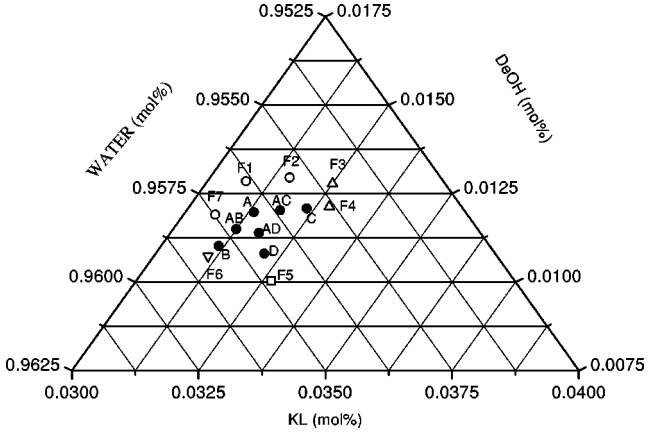

FIG. 1. Surface of the phase diagram of the mixture KL/DeOH/water at $T=23\,^\circ$C. The symbols ●, △, ▽, ○, and □ represent the N_c, ISO+L_α, ISO, N_d, and L_α phases, respectively.

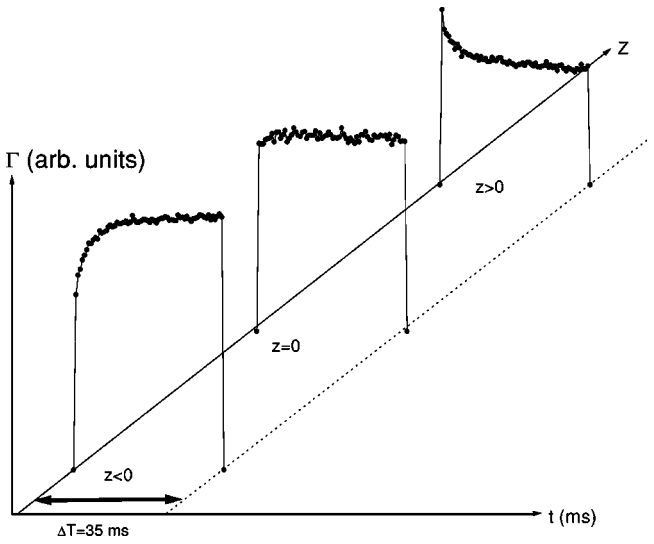

FIG. 2. Time evolution of the absolute optical transmittance in three successive positions of the sample along the z axis. Sample *AD*, $T=23\,^{\circ}\mathrm{C}$.

$H_2 \sim 1$ kG is present. This field, which keeps the same direction of the former H_1, will keep the orientation of the sample during the measurements. The data acquisition is made with temporal resolution, and the signal's temporal evolution is measured. Details about the experimental setup were presented in Ref. [16].

IV. RESULTS AND DISCUSSION

The N_c domain of the phase diagram presented in Fig. 1 is surrounded, in the top-left frontier, by a discotic nematic phase (samples *F1*, *F2*, and *F7*) [18]; in the top-right frontier by a two-phase region constituted by the coexistence of lamellar and isotropic phases (samples *F3* and *F4*); in the bottom-right frontier by a lamellar region (sample *F5*); and in the bottom-left frontier by an isotropic region (samples *F6*).

In the *Z*-scan experiment, due to the presence of a mechanical chopper in the laser beam trajectory, the incident beam has (in time) a square-wave-type profile. Depending upon the sample's position with respect to the focus of the beam, the detected transmittance (also called the time evolution of the detected signal) has its shape modified by the sample with respect to the original square-wave type. Figure 2 presents three typical profiles of the detected signal as a function of time in three positions of the sample with respect to the laser beam focus (at $z=0$), along the z axis. With the measured functions $\Gamma(z,t)$ it is possible to calculate the normalized transmittance $S(z)$. Figure 3(a) shows a typical *Z*-scan curve of the lyotropic mixture in the calamitic nematic phase with an incident power $P=119$ mW on the sample and $\Delta t=18$ ms laser pulses. Equation (2) is used to fit the experimental data to obtain the parameter θ [solid line in Fig. 3(a)]. A systematic deviation of the fitted curve from the experimental data is observed specially for large values of $|z|$. In the fitting procedure, the parameter θ controls first the peak-to-valley amplitude ΔS_{pv}, and, second, the asymptotic behavior at large values of $|z|$. Our results show that the experimental values of $S(z)$ decrease with a smaller rate

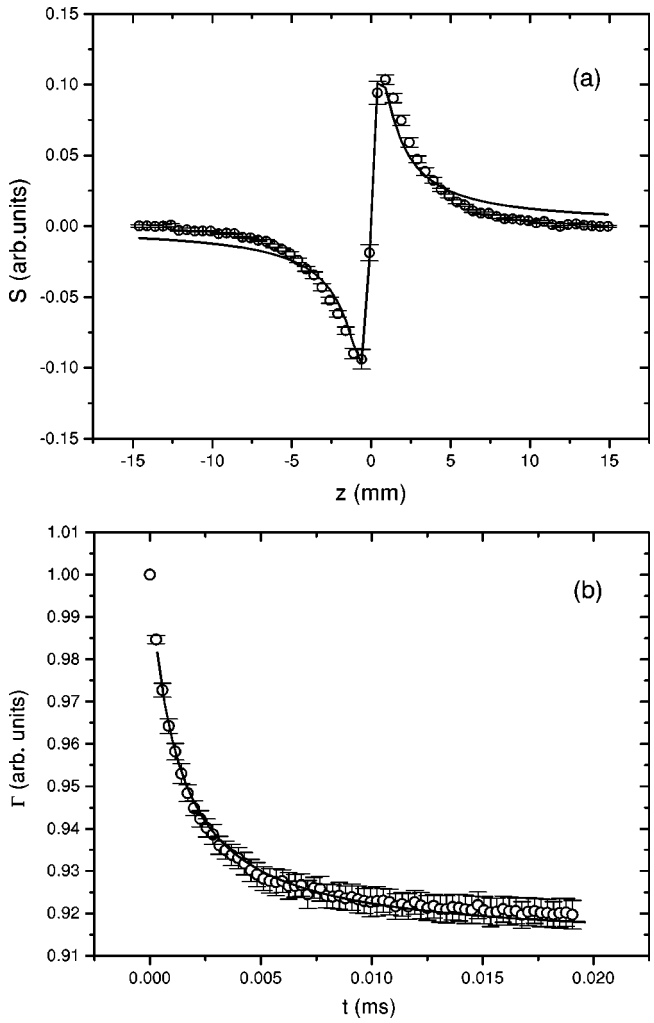

FIG. 3. Typical *Z*-scan transmittances. Sample *AD*, $T=23\,^{\circ}\mathrm{C}$. The nematic director is parallel to the incident electric field. (a) Normalized transmittance $S(z)$. The solid line is a best fit to Eq. (2). (b) Time evolution of the detected signal, $\Gamma(z=0.75\,\mathrm{mm},t)$. The solid line is a best fit to Eq. (4).

(with respect to the sample position) near the focus ($|z| \lesssim 3.5$ mm), and with a larger rate in the far field ($|z| \gtrsim 3.5$ mm), when compared with the fitted curve. This result seems to indicate that two thermal behaviors, with different thermal response times, should be present in the lyotropic sample, depending on the sample position with respect to the focus of the Gaussian-shaped beam. The heat conductivities could be temperature dependent, since the micelles change their shape anisotropy as a function of temperature [19]. We will return to this point later on. A typical set of data of $\Gamma(z=0.75\,\mathrm{mm},t)$ is presented in Fig. 3(b). Equation (4), with the value of θ previously obtained, is used to fit the experimental data and obtain the parameter t_c. The error bars in Fig. 3 also take into account the reproducibility of the experiments. This procedure enables us to calculate k and dn/dT for each sample investigated in different experimental conditions, with the electric field of the laser beam parallel or perpendicular to the sample director **n**. These values are presented in Table II. The value of the linear absorption coefficient, measured independently with a photospectrometer, is $\alpha=(4.4\pm0.1)\times10^{-2}\,\mathrm{cm}^{-1}$. The errors presented in Table II take into account not only the usual propagation and the

TABLE II. Values of the thermal conductivities and thermo-optical coefficients of the nematic samples, in the parallel (∥) and perpendicular (⊥) orientations of **n** with respect to the electric field of the laser beam.

Sample ↓	$k_{\parallel}$ (W/m °C)	$k_{\perp}$ (W/m °C)	$-dn_{\parallel}/dT$ (10^{-5} °C^{-1})	$-dn_{\perp}/dT$ (10^{-5} °C^{-1})
A	0.16±0.04	0.10±0.03	8.2±2.1	10.6±2.7
B	0.14±0.04	0.10±0.03	13.5±3.4	4.7±1.2
C	0.10±0.03	0.13±0.03	3.6±0.9	4.2±1.1
D	0.23±0.06	0.23±0.06	13.2±3.3	8.7±2.2
AB	0.08±0.02	0.13±0.03	3.9±1.0	4.6±1.2
AC	0.39±0.10	0.63±0.16	30.0±7.5	3.4±0.9
AD	0.12±0.03	0.12±0.03	7.8±2.0	5.0±1.3

reproducibility of the experiments, but also the quality of the fitting. The thermal lens model predicts [8] that $\theta \propto P$. Figure 4 shows the linear dependence of θ with P, with sample *F7* (isotropic phase), in good agreement with the TLM. The same behavior is observed with the nematic samples in both orientational conditions. Let us return to the point of the two possible thermal behaviors pointed out above. It is expected that the sample temperature varies [20] as a function of its position with respect to the focus beam: the closer to the focus, the higher the temperature. Figure 5 shows the data of Fig. 3 with two different fit procedures with Eq. (2). In the first one [Fig. 5(a)], only experimental points near the focus ($|z| \lesssim 3.5$ mm) are used; and in the second one [Fig. 5(b)], data with $|z| \gtrsim 3.5$ mm and $|z| \lesssim 1$ mm, namely, the far field limit, are used. Table III shows the thermal parameters obtained with these two fit procedures. Our results indicate that the thermal parameters obtained in the far field limit are smaller (about 1/2 in the case of the parallel configuration and 1/3.4 in the case of the perpendicular configuration) when compared to those obtained in the position closest to the focus. This result can be due to different aspects of the physics of lyotropics. One of them is the large amount of water present in these systems (see Table I). As the thermal conductivity of water increases with temperature [21], this could be one of the sources responsible for the higher values

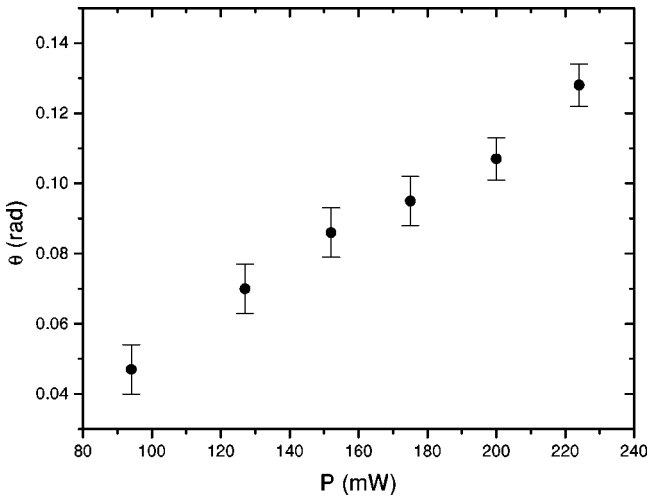

FIG. 4. Dependence of θ on the incident power P. Sample *F6*, $T = 23$ °C.

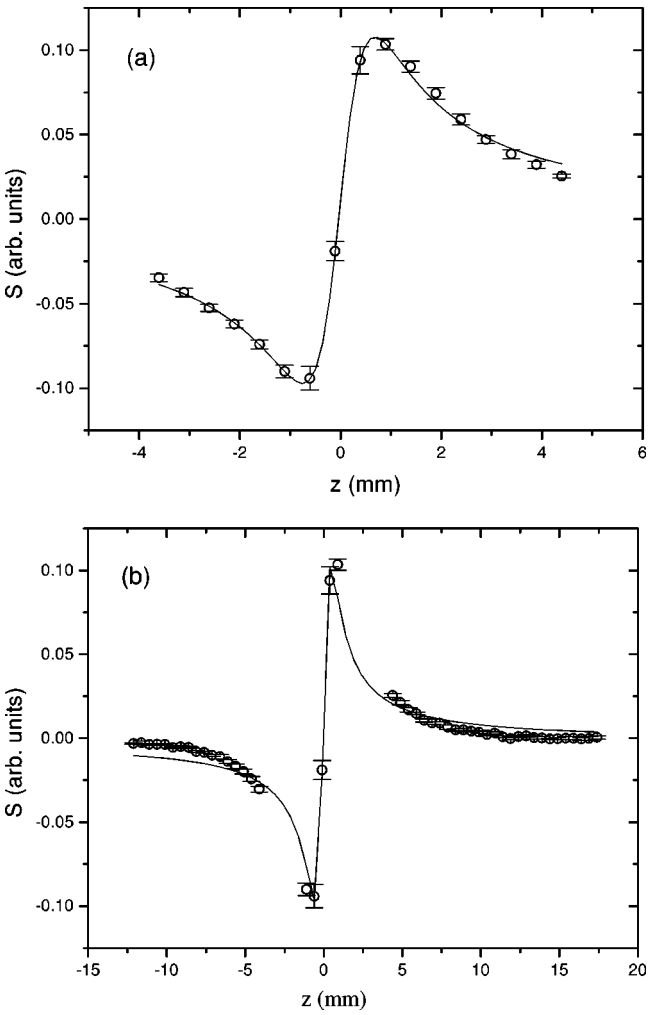

FIG. 5. Data of Fig. 3 with two different fit procedures to Eq. (2): (a) Experimental data with $|z| \lesssim 3.5$ mm. (b) Experimental data with $|z| \gtrsim 3.5$ mm and $|z| \lesssim 1$ mm.

of k obtained with the sample near the beam focus. However, other aspects of the lyotropic system must also be taken into account. It is known that the shape anisotropy of the micelles decreases in the nematic domain as the temperature increases toward the isotropic phase [19]. These changes in the microscopic structure of the micelles as a function of temperature could also modify the thermal properties of the medium. In this framework, the values of the thermal parameters pre-

TABLE III. Values of the thermal conductivities and thermo-optical coefficients of the nematic sample *AD*, in the parallel (∥) and perpendicular (⊥) orientations of **n** with respect to the electric field of the laser beam. Values obtained from the fit of Eq. (2) to the *Z*-scan experimental data, with emphasis on the points near the focus (first row) and in the far field (second row).

	$k_{\parallel}$ (W/m °C)	$k_{\perp}$ (W/m °C)	$-dn_{\parallel}/dT$ (10^{-5} °C^{-1})	$-dn_{\perp}/dT$ (10^{-5} °C^{-1})
$\|z\| \lesssim 3.5$ mm	0.12±0.02	0.12±0.02	7.9±1.0	5.1±0.9
$\|z\| \gtrsim 3.5$ mm and $\|z\| \lesssim 1$ mm	0.07±0.02	0.04±0.02	4.1±0.7	1.5±0.2

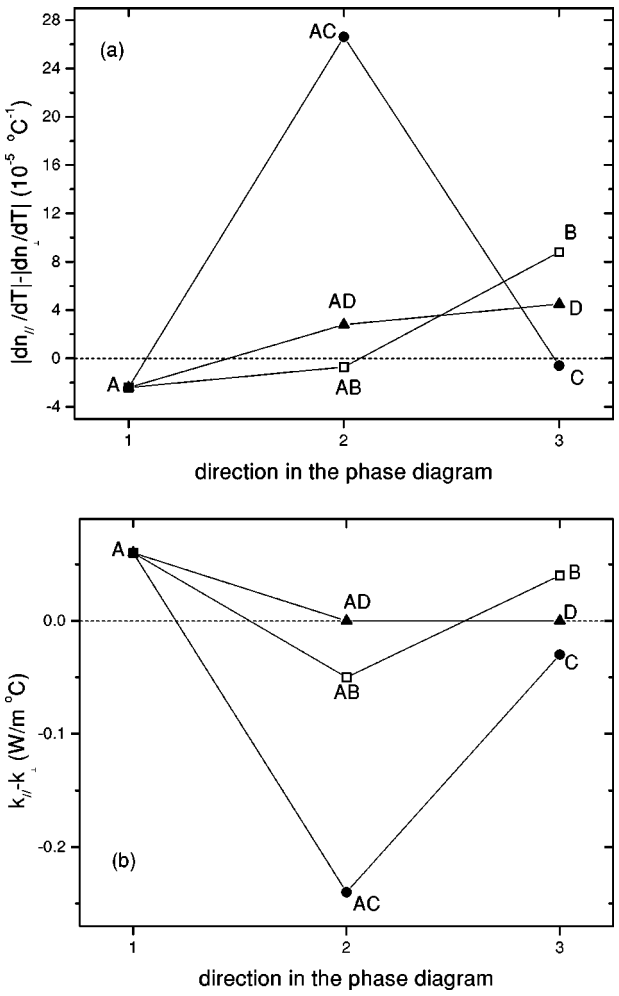

FIG. 6. Anisotropies of the measured parameters of the N_c phase along the three different directions in the phase diagram. Data are extracted from Table II. (a) Thermo-optic coefficients. (b) Thermal conductivities.

sented in Table II must be considered as effective values, closer to those obtained with the sample near the beam focus.

An interesting result of our measurements is the negative sign of both parallel and perpendicular thermo-optic coefficients. It is well known [3,22] that in thermotropic nematic liquid crystals $dn_{\perp}/dT>0$ and $dn_{\parallel}/dT<0$. In the case of lyotropics, however, a different behavior was observed in the mixture decylammoniumchloride-ammoniumchloride-water [23], where the ordinary and extraordinary refractive indices decrease as T increases toward the nematic-to-isotropic phase transition. Our results indicate that the thermo-optic coefficients of the potassium laurate mixture present the same behavior of the decylammoniumchloride mixture. The modification of the shape anisotropy of the micelles as a function of temperature should be responsible for this difference between lyotropics and thermotropics.

Let us now discuss the evolution of the different parameters presented in Table II as we move in the three directions ($A\rightarrow B$, $A\rightarrow C$, and $A\rightarrow D$) in the phase diagram. Figures 6(a) and 6(b) show the evolution of the thermo-optical coefficient and thermal conductivity anisotropies, respectively. The solid and dashed lines in the figures are only guides for the eyes. All the paths start in sample A, near the top-left frontier, in the N_c domain.

A. Direction $A\rightarrow C$

Along this direction, [DeOH]$\sim$1.20 mol %, [KL] and [water] increase, both anisotropies increase (sample *AC*) and then decrease (sample *C*). These results are consistent with the picture in which the micelles increase their shape anisotropy, increasing their dimensions in the plane perpendicular to the amphiphilic bilayer (since the bilayer is almost independent of the concentration of the compounds, being defined essentially by twice the length of the KL molecule). The decrease of the anisotropies observed in Fig. 6 is due to the proximity of the two-phases frontier (ISO$+L_{\alpha}$), with the increase of the water concentration in the mixture. The two-phase region is characterized by the coexistence of the isotropic phase and droplets (with typical sizes of some μm) with a lamellar structure, randomly oriented. The values of the thermal conductivity anisotropies obtained are of the same order of magnitude of those measured by Bento *et al.* [24].

B. Direction $A\rightarrow B$

Along this direction, [KL]$\sim$3.13 mol %, [DeOH] decreases and [water] increases, the thermal conductivity anisotropy decreases, and the thermo-optic anisotropy decreases (sample *AB*) and after changes its sign and increases (sample *B*). It is known that the DeOH molecules are located [25] mostly in the flat part of the micelles. Decreasing the concentration of DeOH leads to a decrease of the shape anisotropy of the micelles (the bilayer remains almost constant during this process); moreover, the increase of the water concentration increases the intermicellar separation, favoring the isotropic phase. These facts should explain the reduction of the thermal conductivity anisotropy from sample *A* to sample *B*, and the thermo-optical anisotropy from sample *A* to sample *AB*. There is, however, an unexpected behavior of the thermo-optic anisotropy from sample *AB* to sample *B*. This result could be related to the proximity of the birefringent N_d phase domain.

C. Direction $A\rightarrow D$

Along this direction, [water]$\sim$95.68 mol %, [DeOH] decreases and [KL] increases, the thermal conductivity anisotropy decreases, and the thermo-optic anisotropy changes its sign (sample *AD*) and afterward remains almost constant (sample *D*). Along this direction in the phase diagram an increase of the micellar shape anisotropy is expected, until the first-order phase transition $N_c\rightarrow L_{\alpha}$. In principle an increase of the anisotropies is expected, and the micelles tend to collapse in large structures, for which it is more difficult to maintain the original planar orientational geometry with small magnetic fields (as can be used in our experimental setup). This effect seems to be the responsible for the results observed.

V. CONCLUSIONS

Z-scan measurements are performed in ferrolyotropic nematic mesophases at a fixed temperature (in the calamitic nematic phase), but with different relative concentrations. The thermal lens model (TLM) is used to obtain the nonlinear parameters (the thermo-optic coefficients and thermal

conductivities) of the liquid crystals. The fit of the theoretical expressions of the TLM to the experimental data indicates that two thermal behaviors with different nonlinear parameters are present, depending on the heating of the sample. This behavior should be related to the modifications of the micellar shape anisotropy as a function of the sample temperature. The anisotropies of the thermo-optic coefficients and the thermal conductivities could be related to the local order and microscopic structure of the nematic phase in different positions of the N_c domain.

ACKNOWLEDGMENTS

FAPESP, CNPq, and PRONEX are acknowledged for financial support.

[1] I. C. Khoo, in *Liquid Crystals: Physical Properties and Nonlinear Optical Phenomena* (Wiley, New York, 1995), and references therein.
[2] C. W. Greef, J. Lu, and M. Lee, Liq. Cryst. **15**, 75 (1993).
[3] C. W. Greef, Mol. Cryst. Liq. Cryst. **238**, 179 (1994).
[4] M. Sheik-Bahae, A. A. Said, T. H. Wei, D. J. Hagan, and E. W. Van Stryland, IEEE J. Quantum Electron. **26**, 760 (1990).
[5] H. Chenming and J. R. Whinnery, Appl. Opt. **12**, 72 (1973).
[6] S. J. Sheldon, L. V. Knight, and J. M. Thorne, Appl. Opt. **21**, 1663 (1982).
[7] S. Wu and N. J. Dovichi, Appl. Phys. **67**, 1170 (1990).
[8] C. A. Carter and J. M. Harris, Appl. Opt. **23**, 476 (1984).
[9] S. E. Bialkowski and A. Carter, Appl. Opt. **36**, 6711 (1997).
[10] F. Jürgensen and W. Schröer, Appl. Opt. **34**, 41 (1995).
[11] I. Jánossy, L. Csillag, and A. D. Lloyd, Phys. Rev. A **44**, 8410 (1991).
[12] I. Jánossy and T. Kósa, Opt. Lett. **17**, 1183 (1992).
[13] *Magnetic Fluids and Applications Handbook*, edited by B. Berkovski and V. Bashtovoy (Begell House, Wallingford, 1996).
[14] F. Brochard and P. G. de Gennes, J. Phys. (France) **31**, 691 (1970).
[15] A. M. Figueiredo Neto and M. M. F. Saba, Phys. Rev. A **34**, 3483 (1986).
[16] S. L. Gómez, F. L. S. Cuppo, A. M. Figueiredo Neto, T. Kósa, M. Muramatsu, and R. J. Horowicz, Phys. Rev. E **59**, 3059 (1999).
[17] L. C. Oliveira, T. Catunda, and S. C. Zilio, Jpn. J. Appl. Phys. **35**, 2649 (1996).
[18] Taking into account the topology of the known phase diagrams of lyotropic nematics, a biaxial nematic phase is expected to be present between the N_c and N_d phases. See, for example, A. M. Figueiredo Neto, in *Phase Transitions in Complex Fluids* (Ref. [19]).
[19] A. M. Figueiredo Neto, in *Phase Transitions in Complex Fluids*, edited by P. Tolédano and A. M. Figueiredo Neto (World Scientific, Singapore, 1998), p. 151.
[20] P. Jägemalm, D. S. Hermann, L. Komitov, and F. Simoni, Liq. Cryst. **24**, 335 (1998).
[21] *CRC Handbook of Chemistry and Physics*, 79th ed., edited by D. R. Lide (CRC Press, Boca Raton, FL, 1998), pp. 6–177.
[22] F. Simoni, Liq. Cryst. **24**, 83 (1998).
[23] T. Haven, K. Radley, and A. Saupe, Mol. Cryst. Liq. Cryst. **75**, 87 (1981).
[24] A. C. Bento, A. J. Palangana, L. R. Evangelista, M. L. Baesso, J. R. D. Pereira, E. C. da Silva, and A. M. Mansanares, Appl. Phys. Lett. **68**, 3371 (1996).
[25] Y. Hendrikx, J. Charvolin, and M. Rawiso, Phys. Rev. B **33**, 3534 (1986).